Forschungszentrum Karlsruhe
Technik und Umwelt
Wissenschaftliche Berichte
FZKA 5956

Simulation Experiments on the Spreading Behaviour of Core Melts: KATS-6 (1-dim spreading of a low superheated iron melt into a dry channel)

G. Fieg, F. Huber, H. Werle

Institut für Neutronenphysik und Reaktortechnik
Institut für Reaktorsicherheit
Projekt Nukleare Sicherheitsforschung

August 1997

Forschungszentrum Karlsruhe
Technik und Umwelt

Wissenschaftliche Berichte

FZKA 5956

Simulation Experiments on the Spreading Behaviour of Core Melts: KATS-6 (1-dim spreading of a low superheated iron melt into a dry channel)

G. Fieg, F. Huber, H. Werle

Institut für Neutronenphysik und Reaktortechnik
Institut für Reaktorsicherheit
Projekt Nukleare Sicherheitsforschung

Forschungszentrum Karlsruhe GmbH, Karlsruhe
1997

Forschungszentrum Karlsruhe GmbH
Postfach 3640, 76021 Karlsruhe

Mitglied der Hermann von Helmholtz-Gemeinschaft
Deutscher Forschungszentren (HGF)

ISSN 0947-8620

ABSTRACT

In future Light Water Reactors special devices (core catchers) might be required to prevent containment failure by basement erosion after reactor pressure vessel meltthrough during a core meltdown accident. Quick freezing of the molten core masses is desirable to reduce release of radioactivity. Several concepts of core catcher devices have been proposed based on the spreading of corium melt onto flat surfaces with subsequent water cooling.
Therefore a series of experiments to investigate high temperature melt spreading on flat surfaces has been carried out using alumina-iron thermite melts as a simulant. The oxidic and metallic phases of the melt are separated and spread on different surfaces. The influence of a shallow water layer on the surface onto the spreading behaviour has also been studied.
In KATS-6 the spreading of an oxidic and metallic melt at low superheat temperatures into one-dimensional dry channels have been planned. During conduct of the experiment it turned out that for the oxidic melt a superheating temperature of less than 100 K was already such low that a relatively strong crust formed near the gate inside the container. Therefore the oxidic melt did not spread when the gate opened to the spreading channel. The spreading of the iron melt, which had a superheat temperature of 200 K did not vary much compared to a higly superheat melt.

Simulationsexperimente zum Ausbreitungsverhalten von Kernschmelzen: KATS-6

ZUSAMMENFASSUNG

Für zukünftige Leichtwasserreaktor-Kraftwerke werden spezielle Einbauten (Kernfänger) erforderlich sein, um das Containment-Versagen infolge von Erosion des Fundamentes bei einem Kernschmelzunfall zu verhindern. Die geschmolzenen Kernmassen sollen möglichst schnell in einen festen Zustand übergeführt werden, um die Freisetzung von radioaktivem Material zu reduzieren. Einige der vorgeschlagenen Kernfängerkonzepte beruhen auf dem Prinzip, die geschmolzenen Kernmassen auf ebenen Flächen zu verteilen und anschließend mit Wasser zu kühlen.
Es wurde deshalb eine Serie von Experimenten durchgeführt, um das Ausbreiten von Schmelzen mit hoher Temperatur auf ebenen Flächen zu untersuchen. Dabei wurde als Simulationsmaterial eine Thermitschmelze aus Aluminiumoxid und Eisen verwendet. Die oxidischen und metallischen Komponenten werden dabei getrennt und auf verschiedene Ausbreitungsflächen geleitet. Der Einfluß niedriger Wasserschichten auf den Flächen auf den Ausbreitungsprozeß wurde ebenfalls untersucht.
In KATS-6 war die Ausbreitung einer oxidischen und metallischen Schmelze bei niedriger Überhitzung in eindimensionale trockene Kanäle geplant. Wie sich bei der Durchführung des Tests herausstellte, war die Überhitzungstemperatur der oxidischen Schmelze von weniger als 100 K bereits so niedrig, daß sich eine relativ starke Kruste im Bereich des Fensters ausbildete. Beim Öffnen des Fensters zur Ausbreitungsfläche trat die Schmelze nicht aus dem Behälter aus. Im Gegensatz dazu breitete sich die Eisenschmelze, welche etwa 200 K überhitzt war, in den trockenen Kanal aus wie eine stark überhitzte Schmelze.

CONTENTS Page

1. INTRODUCTION

Special devices (core catchers) might be required in future Light Water Reactors to prevent containment failure by basement erosion after reactor pressure vessel meltthrough during a core meltdown accident. It is desirable to cool, preferably freeze, the molten core masses quickly in order to reduce the release of radioactivity and the danger of interaction of the melt with structural materials. This implies that thin layers of corium are formed on these structures. Several concepts of core catchers have been proposed to meet these requirements [1-4].
Also the core catcher foreseen for the European Pressurized Reactor (EPR) is based on these principles [5,6], fig.1. The basic concept of this device is to retain the corium masses in the cavern under the reactor pressure vessel long enough to collect most of the corium inventory after the breach of the pressure vessel. Afterwards a gate opens between the cavern and a spreading compartment, into which the corium melt is released. This gate opens as a result of erosion by the melt and the time period for this process has to be about one hour, which is long enough to gather most of the corium after the breach of the pressure vessel. This time period will also allow an increase of the melt temperature and correspondingly a decrease of viscosity to assure a fast spreading of the melt. The composition of the corium is 180 tons of oxidic melt (UO_2 and ZrO_2) and 120 tons of metallic melt (steel and Zr). Cooling of the melt is foreseen from the top by flooding the melt surface with water after the end of the spreading phase.

Corium melt spreading and subsequent interaction of spread corium with water during flooding are generic problems of the EPR core catcher and similar concepts. Models are under development to describe these phenomena. They have to be verified by experiments. The number of experiments with real molten corium will be limited; therefore, tests with appropriate simulant materials are required.

The spreading of corium onto concrete floors has been investigated theoretically [7,8]. In addition, Susuki et al. [8] conducted several spreading experiments using stainless steel melts to verify their modeling. Moody [9] modeled the spreading of corium melt onto a flat surface with and without overlying water. The MELTSPREAD-1 code [10] has been developed at the Argonne National Laboratory and describes the spreading of melts onto dry and wet surfaces. Malinovic et. al. [11] investigated spreading of thermite melts on dry and wet concrete surfaces and also studied the quenching rates due to overlying water pools. Greene et. al. [12] studied the spreading of a variety of materials onto wet and dry surfaces to derive correlations for spreading rates and lengths.

At Siemens/KWU the CORFLOW code [13] has been developed for EPR core catcher investigations. This code describes the spreading of melts onto dry surfaces and has been verified by low temperature melt spreading experiments at the CORINE facility [13]. In addition, CORFLOW

has to be verified with spreading experiments using higher temperature melts, and this is the main motivation for this series of experiments.
These tests are called KATS-experiments (abbreviation for Karlsruher Ausbreitungsexperimente mit Thermit-Schmelzen, Karlsruhe spreading experiments with thermite melts). Spreading experiments of separated alumina and iron melts on dry surfaces cannot directly simulate the spreading of real corium melts. The goal of these experiments is not to simulate as close as possible the behaviour of a corium melt, but to provide experimental data to validate CORFLOW. Therefore there is no need for a realistic scaling-up of the experimental layout to meet the EPR corecatcher design features. Knowledge of material properties, especially viscosity, for both, the simulant and the real melts is essential for extrapolating the results to reactor conditions using a computer model.
In this report the spreading of an iron melt at low superheat into a dry one-dimensional channel is discussed. The low superheated oxidic melt did not spread after opening of the gate due to crust formation.

2. EXPERIMENTAL SETUP

2.1 Test facility and thermite reaction

. The test rig, fig.2, consists of a large reaction crucible for thermite to generate molten alumina and iron, two containers under the crucible to gather the separated melts and the spreading areas (channels). To avoid thermal attack the crucible wall consists of a ceramic material (mainly magnesia). Fig.3 shows schematically the setup. The thermite powder (300 kg) in the crucible is heated up to about 150 ^{0}C for about 24 hours before ignition to release any moisture. Thermocouples inside the thermite powder and the crucible wall control this heating-up phase. At the bottom of the crucible a nozzle, 40 mm in diameter, is installed to discharge the melt. The opening of the nozzle is performed by a pneumatic device, which is initiated by a central control unit. The thermite powder is ignited electrically at the top center of the load. The reaction time for a 300 kg load lasts about 30 s. A delay time of 10 to 15 s between the end of the thermite reaction and the release is needed to allow outgassing of the melt.The arrival of melt at the nozzle is detected by three thermocouples which are located above the nozzle.
The objective of the KATS-6 experiment was to study the spreading of low superheated oxide and iron melts onto dry surfaces until solidification. Therefore the initial high temperature of the thermite melt had to be lowered. First of all, a certain amount of alumina has been added to the thermite powder inside the reaction crucible. This lowered the temperature of both melts. Yet, the iron melt temperature had still to be lowered by

several hundred degrees. This was done by adding a certain amount of iron material into the iron container. The appropriate amounts of thermite, alumina and iron has been calculated with the EquiTherm code [14]. The result is shown in Table 1. The goal was to achieve a total melt mass of about 300 kg yielding an oxidic and metallic melt of about 150 kg each. In addition to the alumina powder (mesh size 100 mikron), the EquiTherm calculation had also to take into account some eroded wall material: from former tests, especially KATS-3b and -4, an amount of about 12 kg of cordierite material from the oxide container has been eroded. This amount has been added into the EquiTherm-calculation, see Table 1. For the time of preparations and conduct of test KATS-6 the GEMINI-code has not been available to analyze the liquidus-solidus region of the oxidic KATS-melts. From post examinations of oxidic PREMIX-samples conclusions have been drawn that the solidus-liquidus temperature is about 1800 ^{0}C. From these more qualitative considerations the melt temperature of the oxidic melt has been chosen between 1950 and 2000 ^{0}C. Yet, GEMINI calculations [15] which have been conducted at a later time, showed that the liquidus temperature is 1925 ^{0}C, which meant that the superheat of the oxidic melt has been less than 100 K. This was the reason why the oxidic melt did not spread onto the surface at the time when the gate opened: A relatively strong crust formed inside the container. As to the iron melt, an amount of 21 kg iron bars have been introduced into the iron container to decrease the melt temperature further down to 1700 ^{0}C. The necessary time for to melt these iron bars has been estimated to be about 7 s.
Practical immediately during the thermite reaction the two phases of the melt, oxide and metal, separate in the crucible and the iron melt pours firstly out of the nozzle after opening. The metallic and oxidic melts are gathered in the two separate containers before spreading into the channels is initiated. The iron melt container is positioned under the nozzle outlet. Under the chosen experimental conditions the pouring takes about 8 s for the iron melt. Once the metallic melt is exhausted, the jet is guided into the second container by a movable chute. The containers are insulated with cordierite plates (52% SiO_2, 37% Al_2O_3, 6.5% MgO) with an open porosity of 23%. This material is highly resistant to temperature shocks and erosion due to high temperature melt jets. Some wall material of both containers is dissolved into the melts because of the low melt temperature of cordierite (1600 ^{0}C). Due to incomplete chemical reaction and wall erosion the the oxidic melt is composed of about 85 weight% Al_2O_3, 5-10 weight% SiO_2 and about 5 weight% FeO.

The quality of separation of the two melt phases depends strongly on the time, when the jet is guided from the iron container into the oxide container via the movable chute. The time to move the chute is calculated under the assumption that the nozzle diameter does not increase due to material erosion. Furthermore, for a short time interval a mixture of oxidic and metallic melt may flow through the nozzle. Therefore a complete separation was not possible with this method. In the case that the jet is

directed too late into the oxidic container some oxidic melt is gathered in the container for the iron melt. Except for the small resulting higher pressure head in the container the spreading of iron is not disturbed by the presence of this oxide. Yet, in the case that the jet is directed too early into the oxide container, some iron gathers at the bottom of the oxide container and spreads onto the surface together with the oxide melt. To minimize this risk a "swamp" volume of more than 7 liters (equivalent to more than 40 kg of iron) for this excess iron melt in the oxide container has been foreseen.

The gates between melt containers and spreading channels were closed with ceramic plugs made of magnesia. They are of a conical form with the smaller dimensions towards the container holding the melt. The reason for this conical form is to insure a safe opening at the moment when the plugs are released by a pneumatic and mechanical spring device. Fig. 4 shows the dimensions of container, gate and spreading channel for the iron melt. The dimensions of both containers, gates and spreading channels are listed in Table 1. This table lists also the main parameters at the onset of spreading.

The spreading channels are constructed of concrete covered with cordierite plates and additionally with ceramic (an alumina/silica mixture) as in the preceeding tests KATS-3b, -4 and -5 [16,17]. The channels have been adjusted carefully with a slope of less than 1mm over a length of 1 m against the horizontal.

2.2 Instrumentation and Data Recording

Due to the fact that the oxide melt did not spread as mentioned in the former chapters, in the following only the instrumentation for the iron spreading channel is described. During the spreading process the temperature of the iron melt is measured with W-Re thermocouples at three different axial positions in the channel (0.3m,3.3m and 6.3m), with the thermocouple junction level 10 mm above the channel floor. Thermocouples of type K (1 mm outer diameter) are positioned at different vertical positions (5, 15,25 and 35 mm above the floor level) at different positions in the channel, table 2. These thermocouples have been installed to indicate the arrival time of the melt. Fig. 5 shows the positions and identification of the single measuring points. In addition to these thermocouples several video-cameras, positioned at different locations, recorded the spreading process.

The measured and amplified signals were recorded using a digital 32 channel transient recording system. A sampling rate of 1kHz per channel was applied leading to an overall recording time of 256 s. The transient recorder was started with the command to open the gate between the iron container and spreading channel. After conduct of the experiment the recorded data were transferred and stored on a disk. The evaluation is

done with a special computer program supplied together with the transient recording system. For synchronisation reasons of the different video recorders flashlights were triggered together with the commands for thermite ignition and opening of the gates.

2.3 Control System

The commands during conduct of the tests (thermite ignition, tapping the crucible orifice, moving the chute and opening the gates) are controlled by an electronic control system. The duration for the thermite reaction and hence the tapping of the orifice has been estimated with an established rule of thumb: the reaction front velocity proceeds at 25 to 30 mm/s for the thermite powder as used in these tests. The time for the iron melt to flow out of the reaction chamber have been calculated with Torricelli's law. From this the time to move the chute leading the oxidic melt into the oxide container has been estimated. The opening of the gates are initiated after the melt was released from the reaction crucible. Table 3 shows the timing of the different commands during conduct of the experiment. A longer time period for the iron melt in the container was necessary to melt the additional iron bars has been taken into consideration.

3. RESULTS

As already mentioned in the preceeding chapter, the oxide melt did not spread opnto the channel after opening the gate. Therefore data are only available for the iron spreading test which is described in the following.
Fig. 6 shows the traces of all three W-Re thermocouples at three axial positions (0.3 m, 3.3 m and 6.3 m, measured from the gate). The temperatures close to the gate at 0.3 m and at 3.3 m distance are 1670 ^{0}C and 1700 ^{0}C, close to the calculated original temperature. Further downstream at 6.3 m the temperature was appreciably lower, 1370 ^{0}C, which is below the freezing point temperature of iron. One has to take into account that the response time of these relatively large C-type thermocouples is about 4 seconds. At the time when the thermocouple reading reached its asymptotic value, the melt already arrived its final spreading at 8.5 m. Table 4 shows the arrival times at the type K thermocouples locations. Included are also the average velocities as calculated from the thermocouple readings. Figs. 7-10 show the corresponding transient registrations for these thermocouples. Fig. 11 shows the arrival times of the iron melt at different axial positions and different vertical heights. The response time of these thermocouples is about 50 ms. Any systematic errors due to this response are cancelled in evaluating leading edge velocities because time differences are used between two different thermocouple readings.

The pouring rate of the iron melt into the spreading channel can be calculated according to Torricelli's law including a pouring factor of 0.6 for the given geometry [18]. The pouring rate starts with 17.6 l/s at the onset of opening the gate and decreases linearly to zero at 4.3 seconds. The maximum spreading velocity is 2.68 m/s at the beginning and decreases steadily with time. The transient spreading of the iron melt can also be analyzed with the videorecordings. Fig. 12 shows these results together with the K-type thermocouple recordings at 5 mm vertical positions. The final spreading length is 8.77 m. After cooling down to ambient temperature the iron slag shrinked in axial direction by 140 mm.

Post experimental examination of the iron slag in the channel has been done, fig. 13 shows its axial mass distribution. A total mass of 128.1 kg of iron spread into the channel. The remaining iron is partly found inside the iron container, a larger amount has been gathered in the swamp volume of the oxide container. The initial level height of the iron melt in the container has been calculated according to the iron which was found in the iron container and spreading channel, Table 1. The height of the solid iron slag, fig. 14, is deduced from the axial mass distribution of the solid slag. The average height, calculated from this axial height distribution, is 9.1 mm. Due to different densities between liquid and solid iron a correction has to be done to get the average height of the liquid slag at the time of immobilisation, also the fact of shrinking had to be accounted for. So, at the time of immobilisation the average height was 11.2 mm. The leading edge velocity of the melt and consequently its inertia force is very small towards the end of spreading. The viscosity of liquid iron does not change much with temperature. Immobilisation of the iron is therefore not due to increasing viscosity, but rather correlated to the surface tension of liquid iron.

With a simple analytical expression between the gravitational force of the slag and the surface tension at the front of the slag the melt height can be calculated. When inertia forces can be neglected, which is the case towards the end of spreading, only gravitation and surface tension are the dominating forces and the induced pressures (p) are:

Gravitational head of the melt: $p_g = \rho \cdot g \cdot h$

Surface tension: $p_s = \frac{2 \cdot \sigma}{r}$

h=melt height
r=h/2=curvatore radius at the front
σ=1.45 N/m surface tension of iron at melt temperature
ρ=6300 kg/m^3 specific density of liquid iron

The resulting melt height h at which the two pressures are balancing each other, is:

$h = \sqrt{\frac{4\sigma}{\rho g}} = 9.7mm$, which is in rather good agreement with the experimental value (11.2 mm).

4. SUMMARY

The one-dimensional spreading of an iron melt at low superheat temperature (200K) into a dry one-dimensional channel has been studied. The iron melt spread evenly over a distance of 8.6 m. The average height of the melt was 10 mm. Immobilisation of the iron melt is due to the relatively high surface tension.
The temperature of the oxidic melt has been close to the liquidus temperature. It did not spread into the channel due to early crust formation inside the container.

5. REFERENCES

1. J.D. Fish, M. Pilch and F. Arrellano, "Demonstration of Passively-Cooled Particle-Bed Core Retention," Proceedings of the 5th Post Accident Debris Cooling Information Exchange Meeting, Karlsruhe, Germany,28-30 June 1982, 319-324

2. H. Alsmeyer et. al., "Improved Containment Concepts for Future Large LWR's," IEA Int. Conf. Technology Responses to Global Environmental Challenges, Kyoto, Japan, 6-8 November 1991, 471-489

3. A. Turricchia, "How to Avoid Molten Core/Concrete Interaction and Steam Explosions," Proc. 2nd Organization for Economic Cooperation and Development Committee on the Safety of Nuclear Installations Specialist's Meeting on Molten Core Debris-Concrete Interaction, Karlsruhe, Germany, April 1992, KfK-Report 5108, 503-518

4. J.M. Seiler, F. Balard, M. Durin, A. Méjane, S. Pigny and I. Szabo, "Conceptual Studies of Core Catchers for Advanced LWR's," Proc. Int. Conf. Design and Safety of Advanced Nuclear Power Plants, Tokyo, Japan, October 25-29, 1992, Vol III, p. 300-327

5. M. Michel et. Al., "EPR Safety Approach and Consideration of Severe Accidents,"Transactions of the ENC '94, Lyon, France, October 2-6,1994, Vol.II,502-506

6. M. Fischer, Siemens/KWU, private communication, May 1996

7. M.S. Kazimi, "On the Liner Failure Potential in MARK-I Boiling Reactors," Nucl. Science and Engineering, **103**, 59-69 (1989)

8. H. Suzuki, T. Mitadera, I. Sakaki and T. Zama, "Fundamental Experiment and Analysis for Melt Spreading on Concrete Floors," Proc. Intern. Conference on Nucl. Energy (ICONE-2), San Francisco, March 21-24, 1993

9. F.J. Moody, "First Order Analyses of Molten Corium Heat Transfer," ANS Proc. 1989 National Heat Transfer Conference, August 6-9, 1989, Philadelphia, PE, 217-224

10. M.T. Farmer, J.J. Sienicki, B.W. Spencer and C.C. Chen, "Status of the MELTSPREAD-1 Computer Code for the Analysis of Transient Spreading of Core Debris Melts," Proc. 2nd Organization for Economic Cooperation and Development Committee on the Safety of Nuclear Installations Specialist's Meeting on Molten Core Debris-Concrete Interaction, Karlsruhe, Germany, April 1992, KfK-Report 5108, 489-502

11. B. Malinovic and R. E. Henry, "Experiments Relating to Drywell Shell-Core Debris Interaction", EPRI-NP 7196L (February 1991)

12. G.A. Greene, K.R. Perkins and S.A. Hodge,"Mark I Containment Drywell-Impact of Core/Concrete Interactions on Containment Integrity and Failure of the Drywell Liner," Proceedings of an International Symposium on Source Term Evaluation for Accident Conditions, Columbus,OH, October 28-November 1, 1985, pp 429, International Atomic Energy Agency, Vienna, (1986).

13. J. M. Veteau and R. Wittmaack, "CORINE Experiments and Theoretical Modelling," FISA-95 Symposium - EU Research on Severe Accidents, Luxembourg, Nov. 20-22, 1995, 271-285

14. M. Steinbrück: EquiTherm-calculations, private communication

15. M. Steinbrück: GEMINI-calculations, private communication

16. G. Fieg, H. Werle, F. Huber, "Simulation experiments on the spreading behaviour of molten core melts:KATS-3b and KATS-4",Forschungszentrum Karlsruhe, Wissenschaftlicher Bericht FZKA 5887, 1997

17 G. Fieg, H. Werle, F. Huber, "Simulation experiments on the spreading behaviour of core melts:KATS-5 (1-dim spreading of an oxidic melt into a dry channel)", Forschungszentrum Karlsruhe, Wissenschaftlicher Bericht FZKA 5920, 1997

18. Dubbel Taschenbuch für den Maschinenbau, Springer Verlag, 17. Auflage, 1990, B52-B53

ACKNOWLEDGMENT:

This work was partly supported by a contract between FZK and EVU/Siemens.

Table 1 Dimensions of oxide and iron melt container, spreading channels, melt levels and masses for KATS-6

	Unit	Oxide	Iron
Container inner width	cm	37.8	17.8
Container inner depth	cm	32.5	32.5
Release gate height	cm	5.0	5.0
Release gate width	cm	34.0	14.0
Channel width	cm	40.0	20.0
Channel length	m	8.5	11.5
Height of melt in container [1])	cm	-	34.2
Melt mass [1])	kg	-	-

[1]) Data derived from post experimental examination

Table. 2 Location of thermocouples in test KATS-6 (Iron melt)

Axial position of thermocouples (m)	Thermocouple # Vertical positions of thermocouples			
	5 mm	15 mm	25 mm	35 mm
0.3	E.TK.0305 E.TW.0305	-	E.TK.0325	-
1.8	E.TK.1805	-	E.TK.1825	E.TK.1835
3.3	E.TK.3305 E.TW.3305	E.TK.3315	E.TK.3325	E.TK.3335
4.8	E.TK.4805	E.TK.4815	E.TK.4825	-
6.3	E.TK.6305 E.TW.6305	E.TK.6315	-	-
7.8	E.TK.7805	E.TK.7815	-	-
9.3	E.TK.9305	-	-	-
10.8	E.TK.10805	-	-	-

TW= C-type thermocouple
TK= K-type thermocouple

Table 3 Time chart of the KATS control system for test KATS-6

Test KATS-6	
Event	Time (s)
Ignition of thermite powder Flashlight #1 Start Videosystem Start Transient Recorder	0
Start of melt release out of crucible	45.0
Start of moving chute	53.0
Chute on end position	55.5
Open gate for oxide melt Flashlight # 2	80.0
Open gate for iron melt Flashlight #3	90.0

Table 4 Arrival times and velocities of iron melt at axial and vertical thermocouple locations in test KATS-6

Axial position of thermocouples (m)	Melt arrival times (s) Melt velocity (m/s) Vertical positions of thermocouples			
	5 mm	15 mm	25 mm	35 mm
0.3	0.33	(no thermocouple)	0.35	(no thermocouple)
	2.68 m/s	-	2.67 m/s	-
1.8	0.89	(no thermocouple)	0.91	0.84
	1.48 m/s	-	1.68 m/s	1.61 m/s
3.3	1.90	1.98	1.80	1.77
	1.02 m/s	1.01 m/s	0.91 m/s	-
4.8	3.37	3.46	3.44	(no thermocouple)
	0.66 m/s	0.66 m/s	-	-
6.3	5.66	5.74	(no thermocouple)	(no thermocouple)
	0.39 m/s	0.40 m/s	-	-
7.8	9.54	9.45	(no thermocouple)	(no thermocouple)
	-	-		-
9.3	-	-	-	-
10.8	-	-	-	-
	-	-		-

The velocities are melt front velocities between two consecutive axial thermocouple positions at identical vertical locations

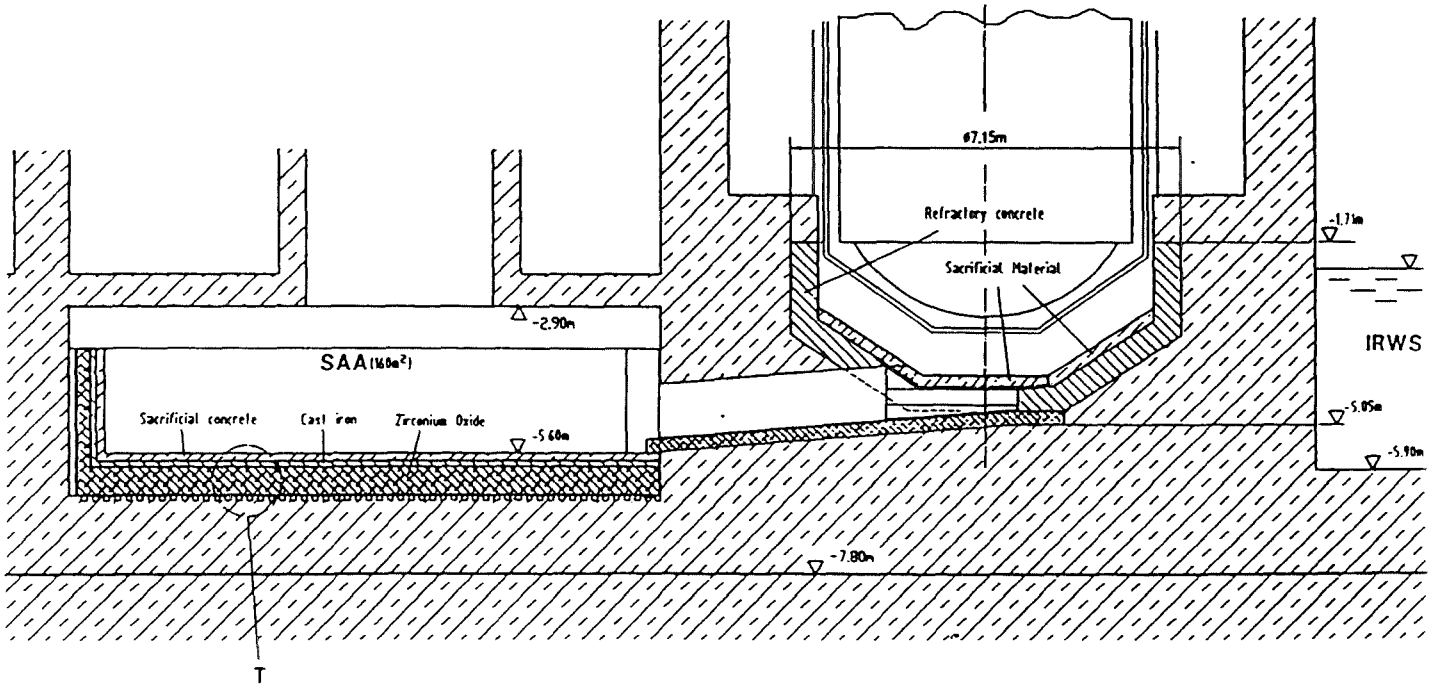

Fig. 1 Improved Reference Concept of the EPR Core-melt Retention System

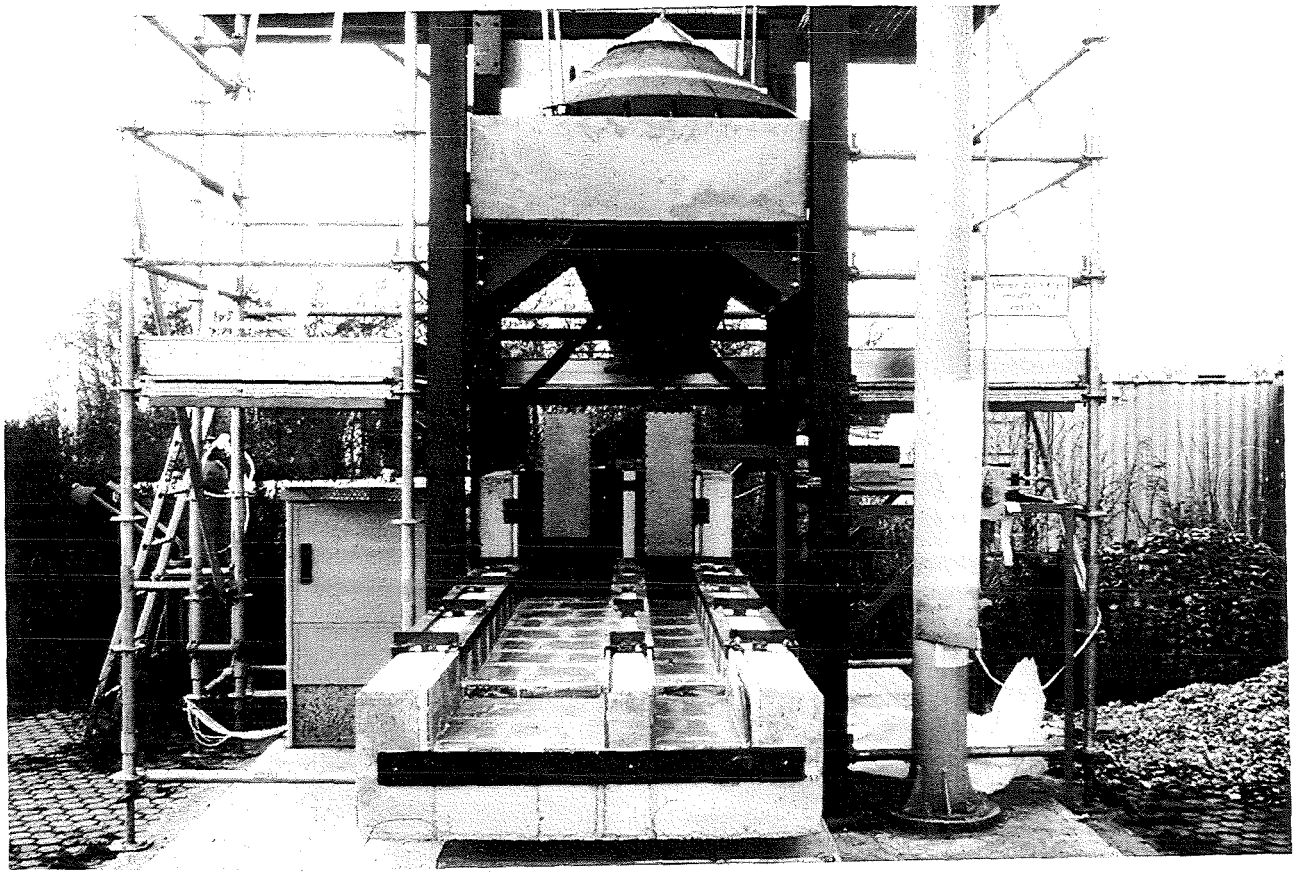

Fig.2 Photo of the KATS Facility

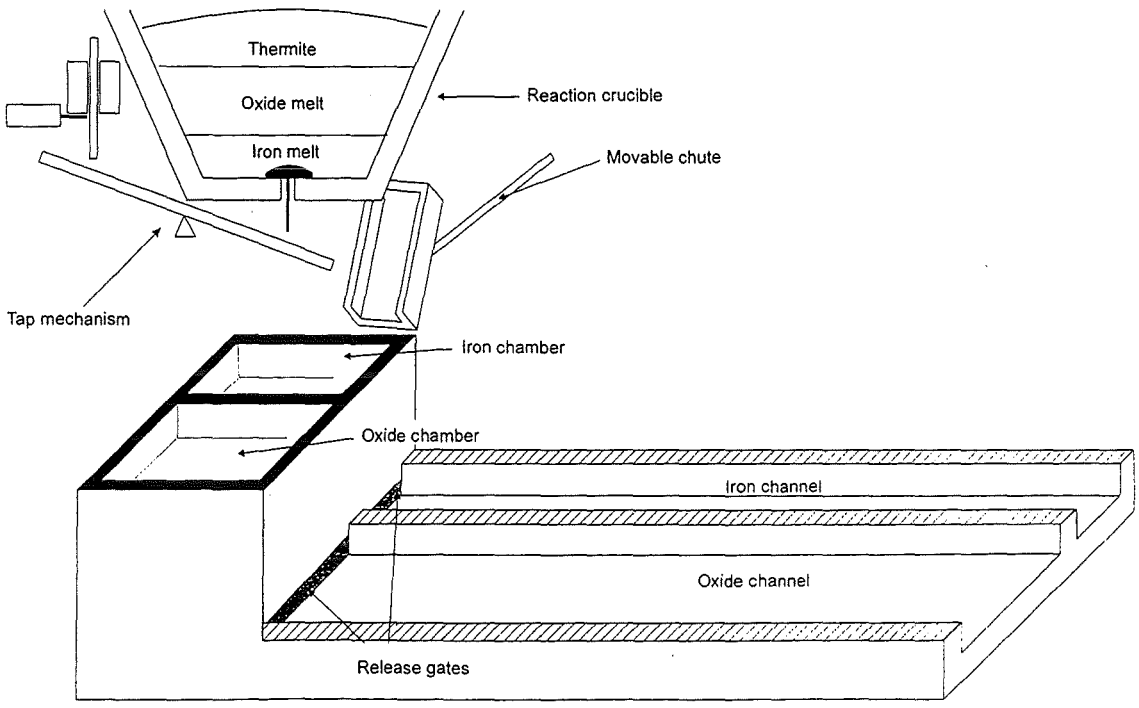

Fig.3 Schematics of the KATS Facility

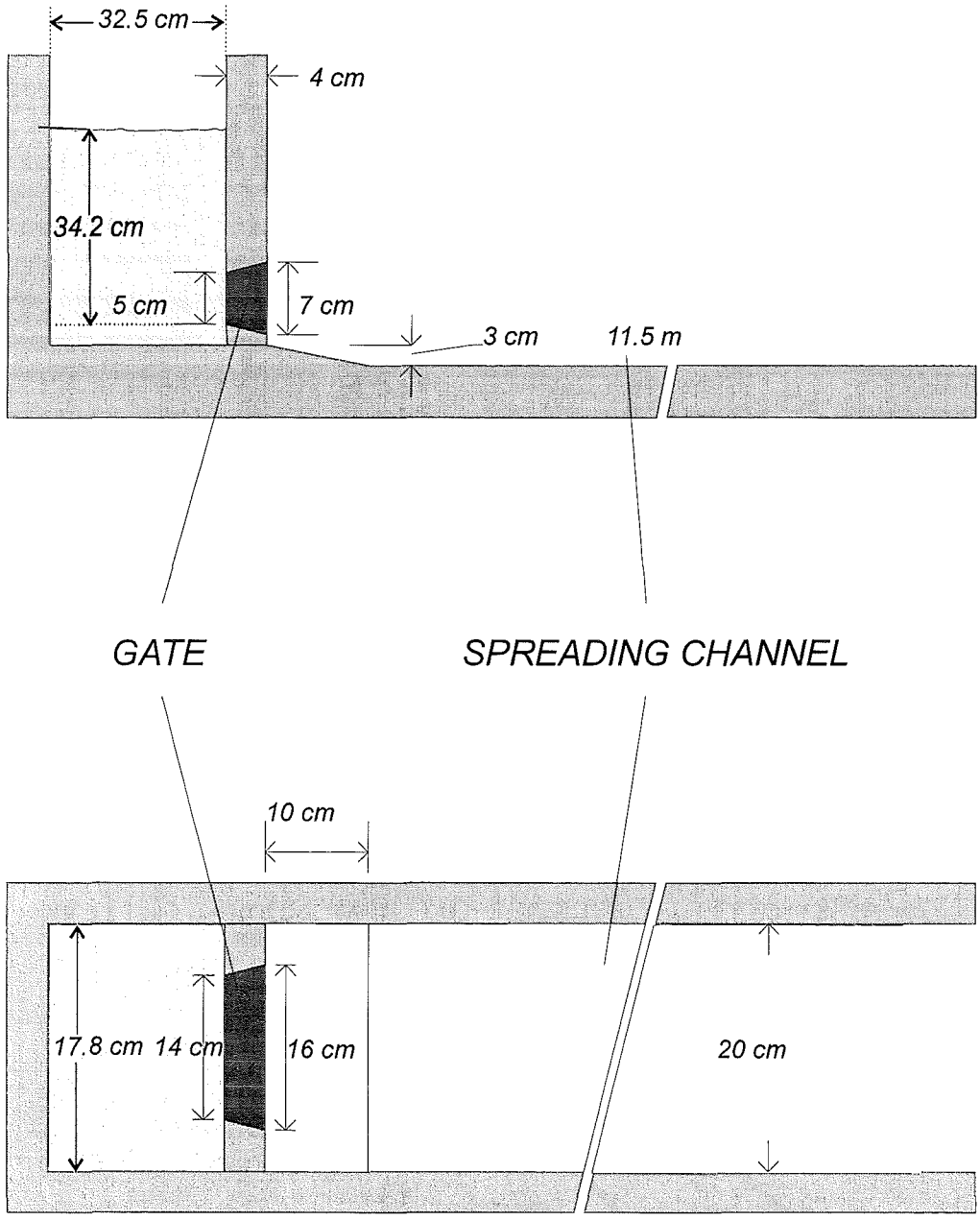

Fig.4 Geometry and dimensions for the spreading of iron melt in KATS-6

Explanation:

TK = K-type thermocouple
TW=C-type thermocouple

0325 =axial position 0.3m , height 25 mm

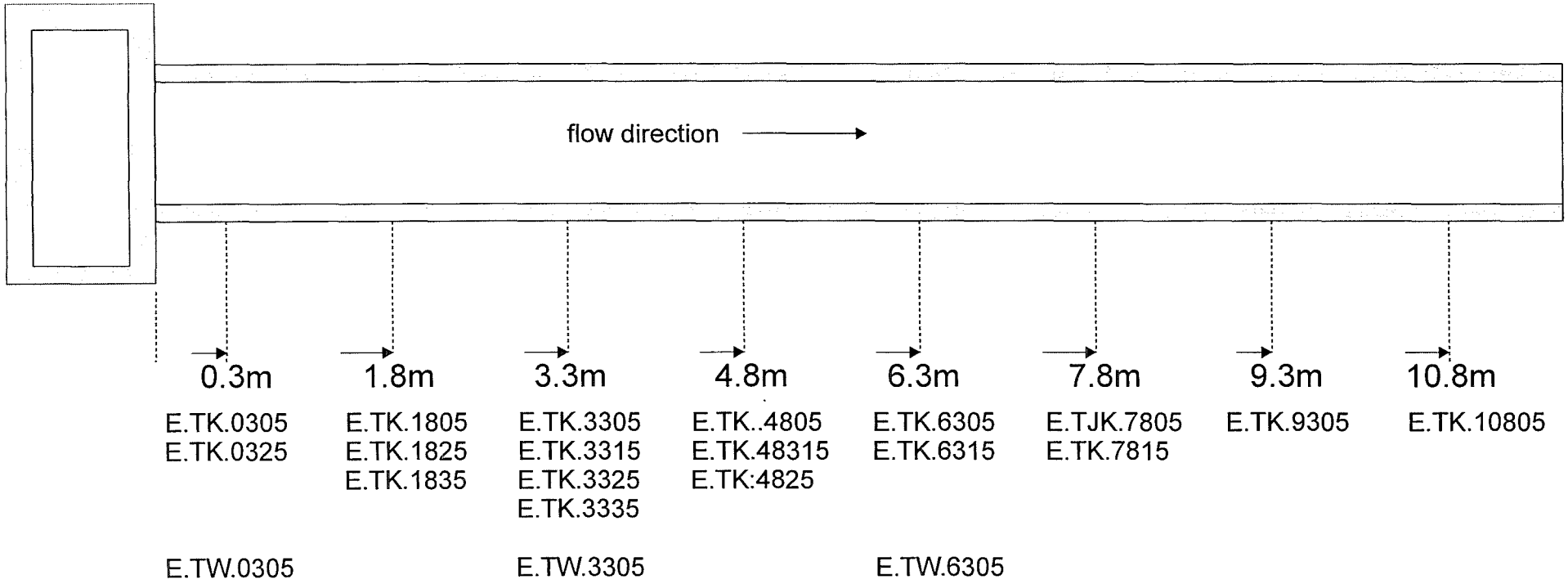

Fig. 5 Test KATS-6, positions of thermocouples in the iron spreading channel

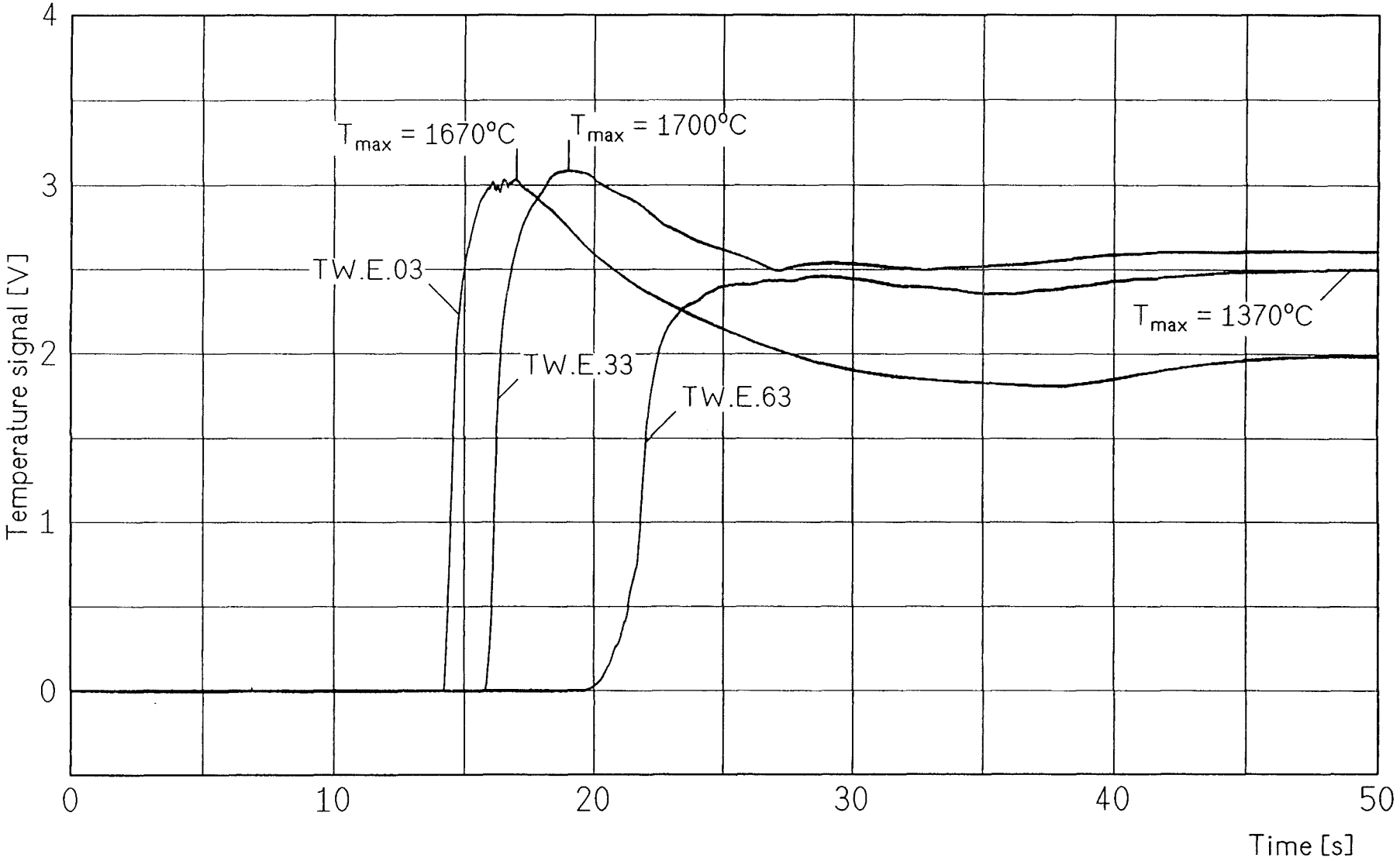

Fig. 6 Test KATS-6 Temperature of the iron melt at three positions

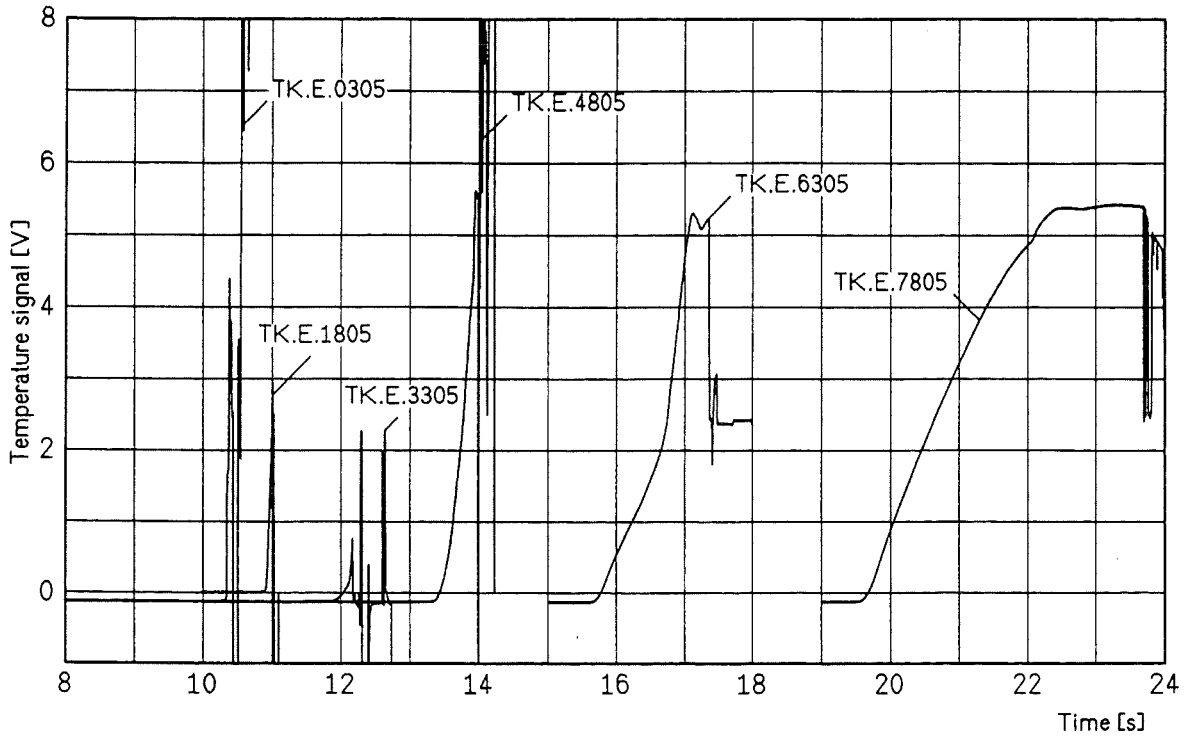

Fig. 7 Test KATS-6 Detection of the iron melt at 5mm height

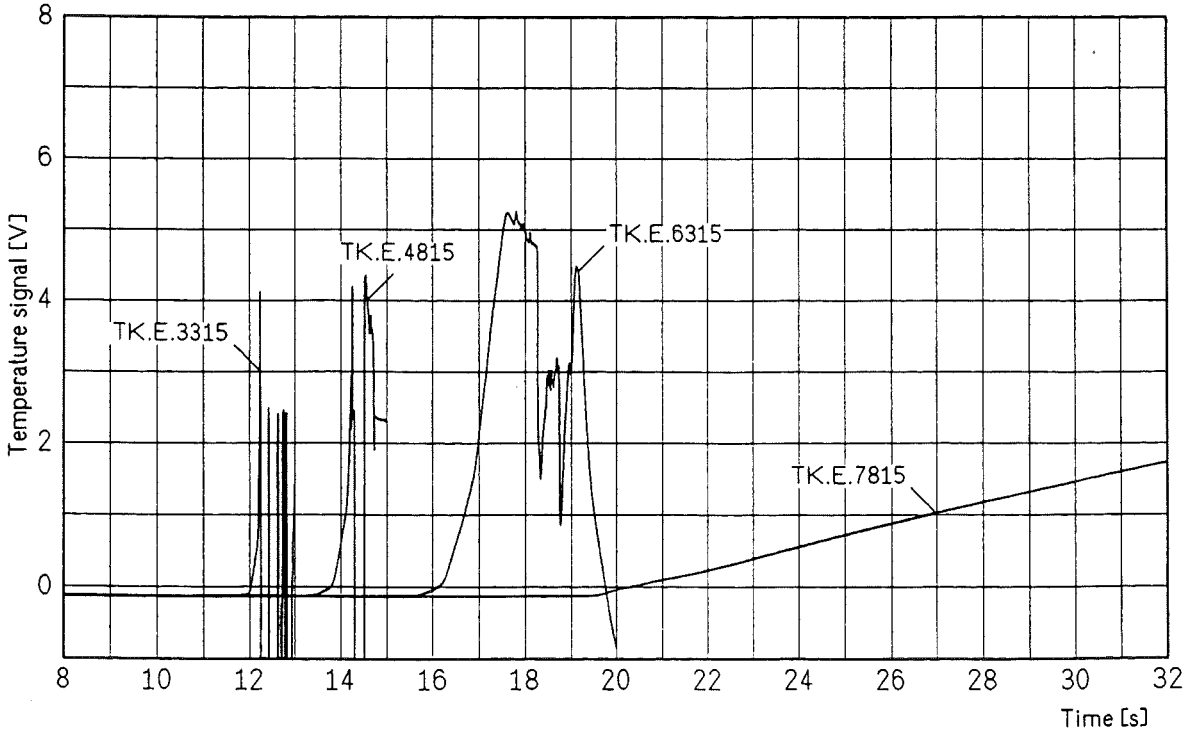

Fig. 8 Test KATS-6 Detection of the iron melt at 15mm height

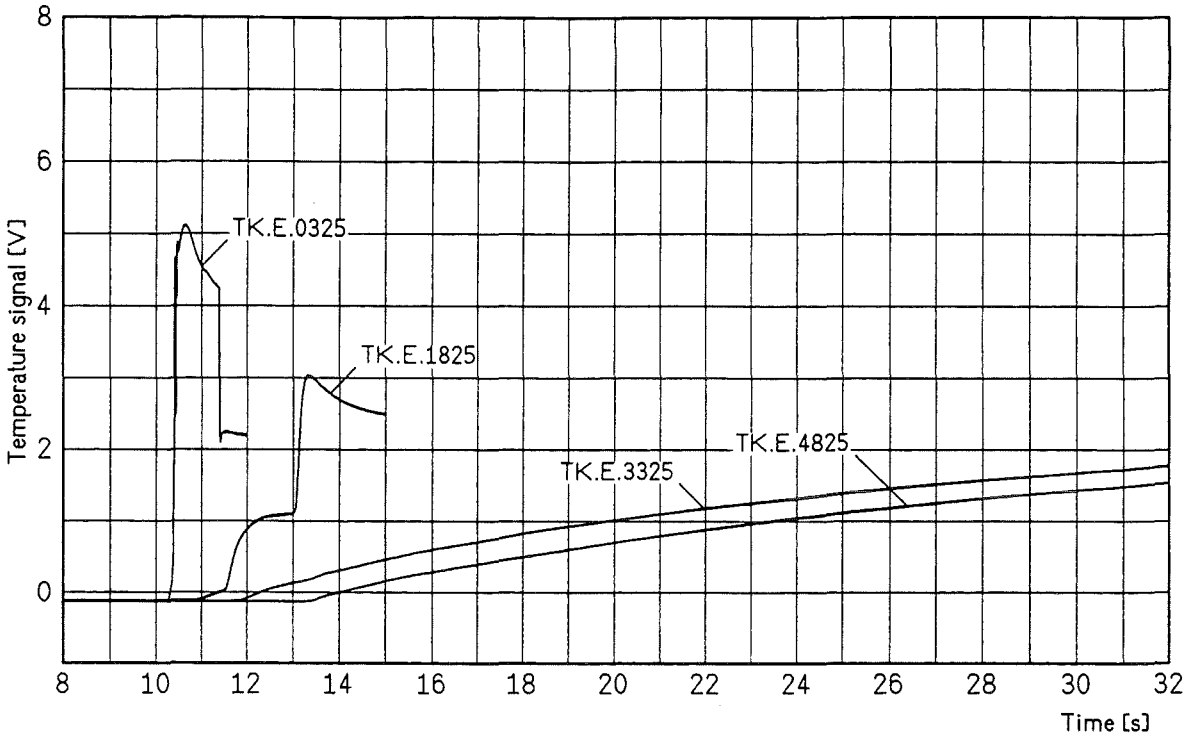

Fig. 9 Test KATS-6 Detection of the iron melt at 25mm height

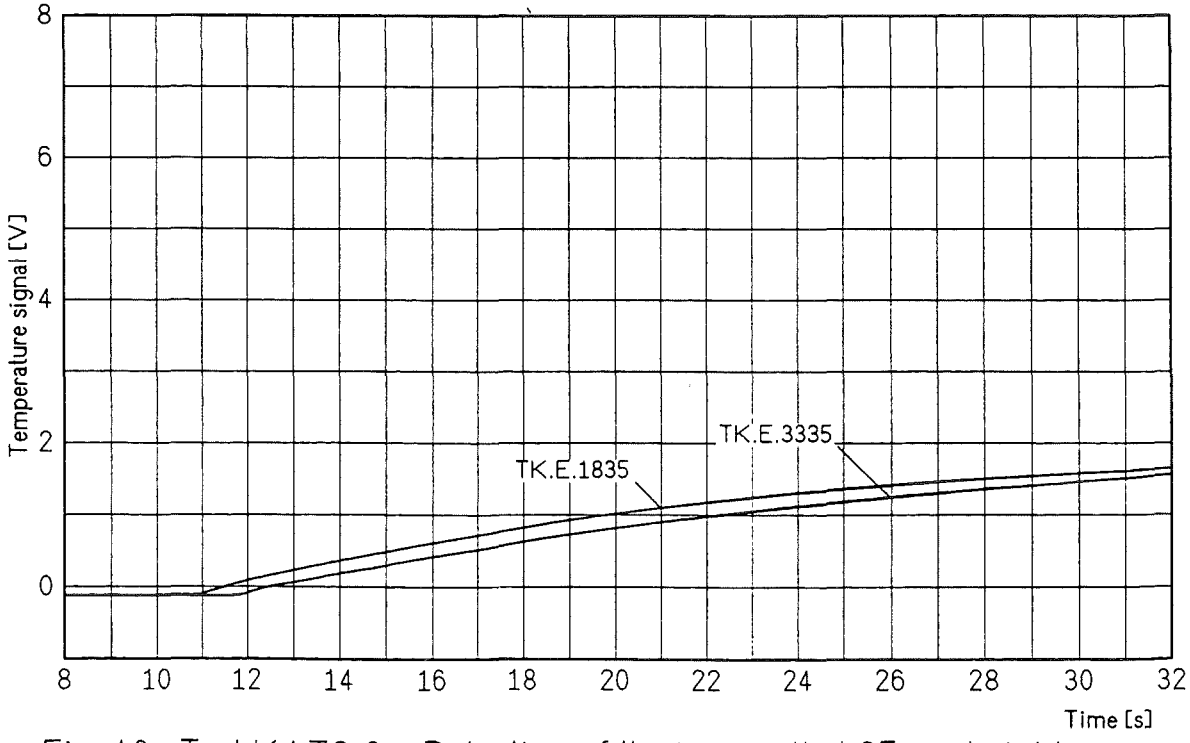

Fig. 10 Test KATS-6 Detection of the iron melt at 35mm height

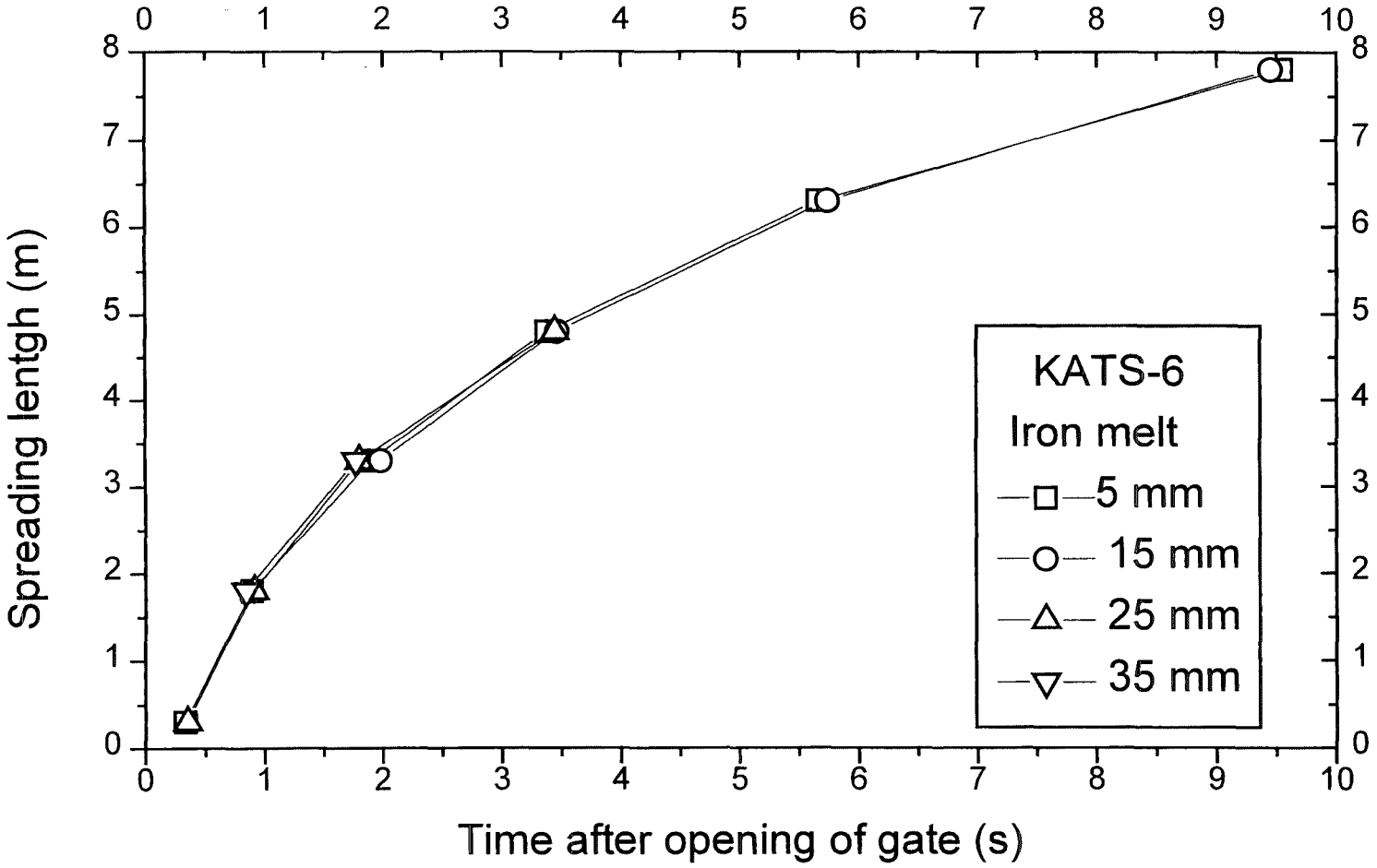

Fig. 11 Transient spreading of iron melt at different vertical locations

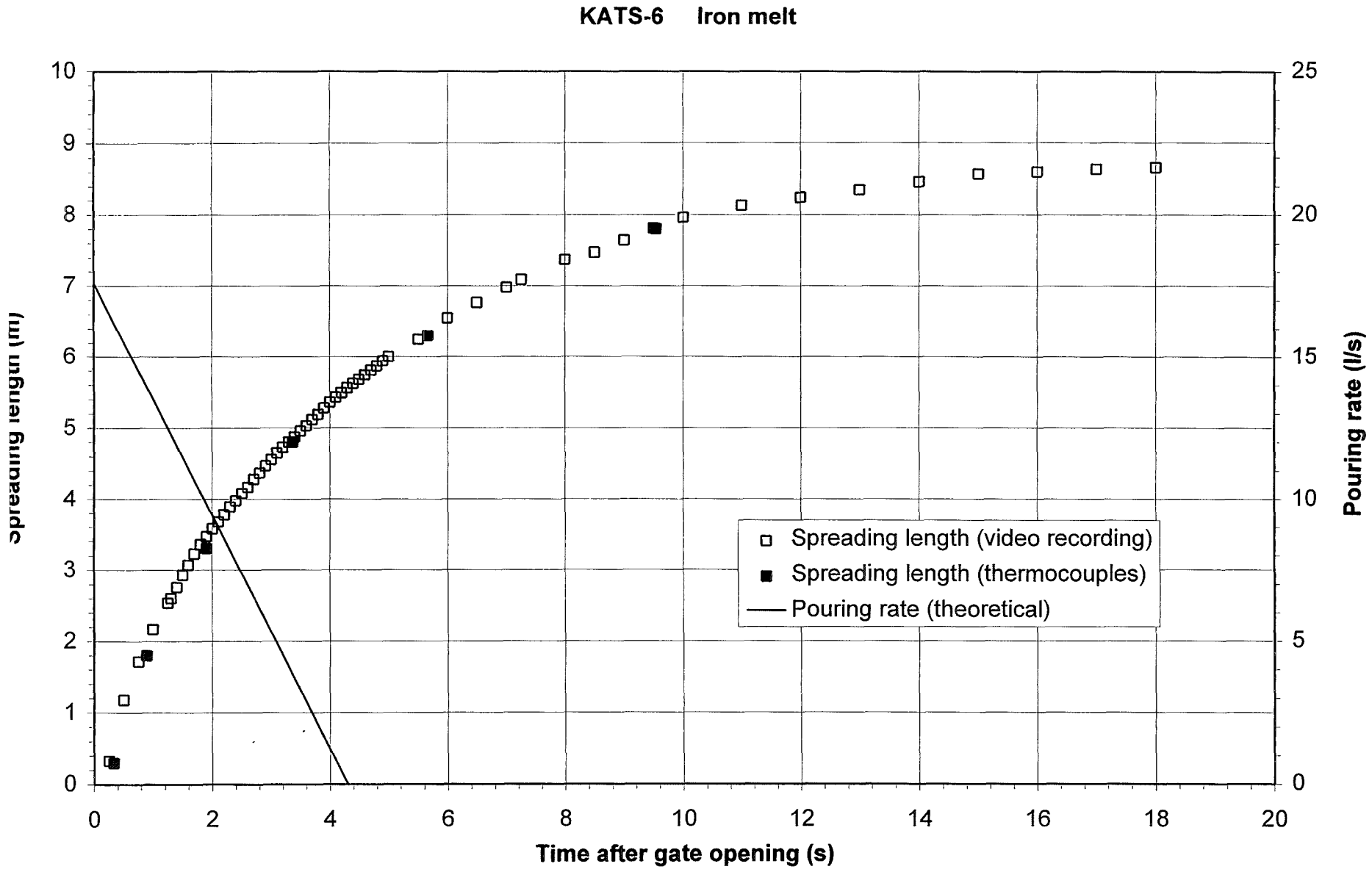

Fig. 12 Transient spreading of iron melt into channel

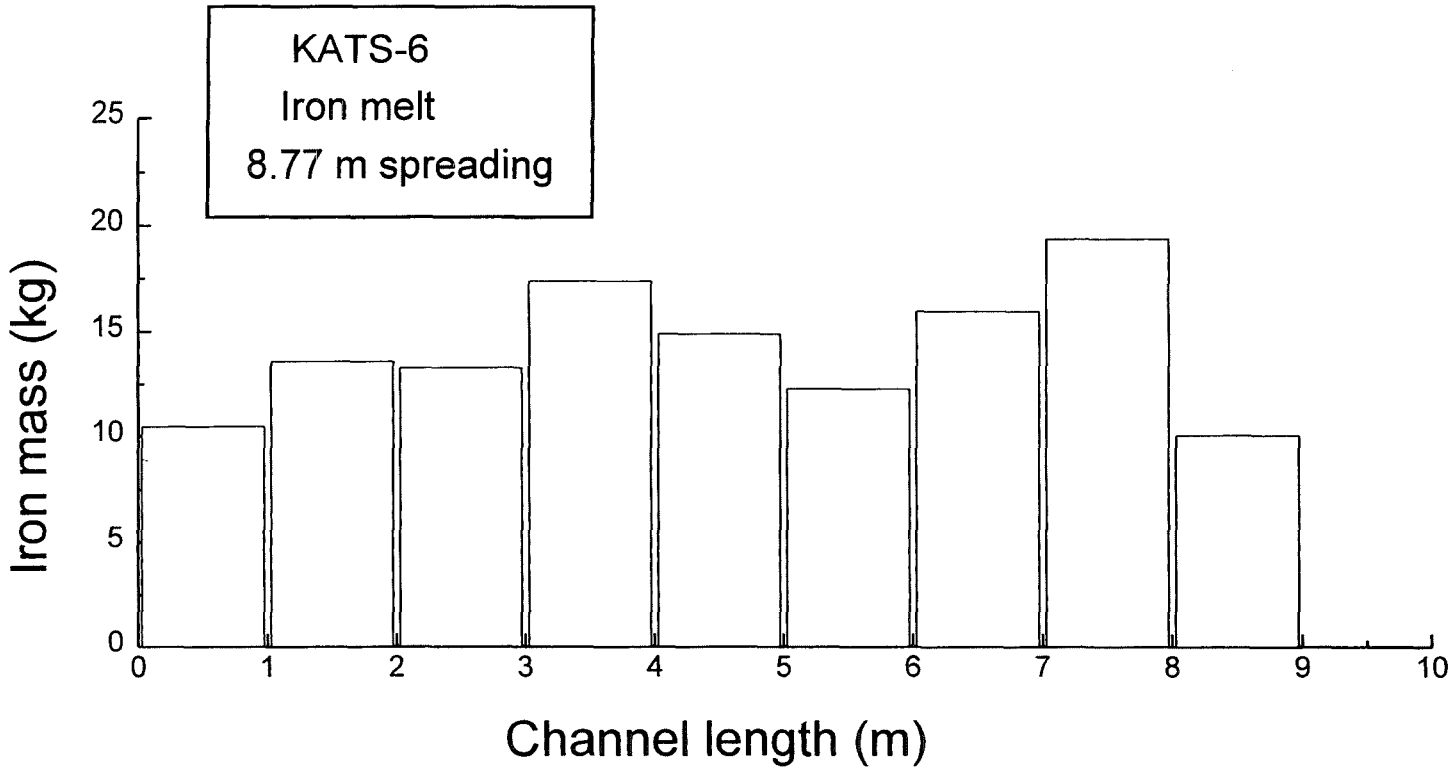

Fig.13 Axial distribution of solidified iron in the channel after spreading

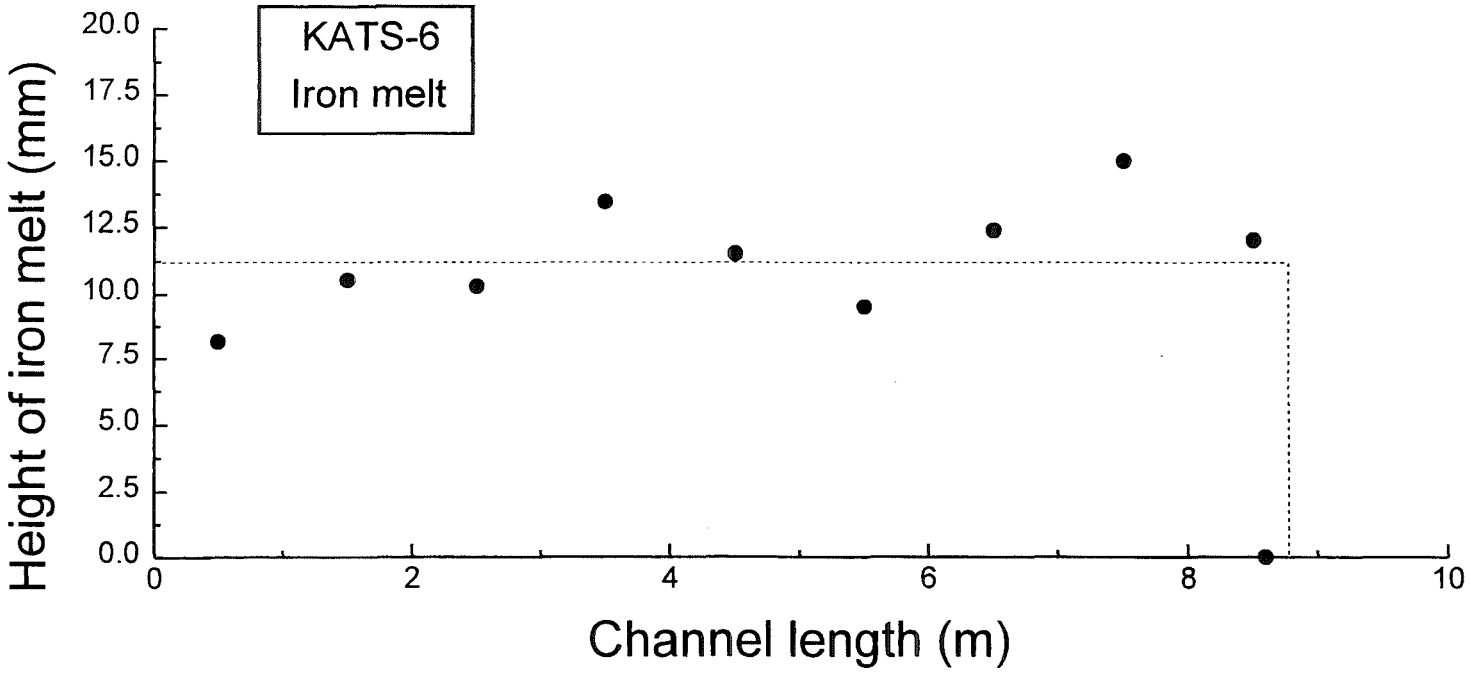

Fig. 14 Height distribution of liquid iron slab at time of immobilization
(Average value is 11.2 mm)